Exponential Growth of Nonlinear Ballooning Instability

P. Zhu, C. C. Hegna, and C. R. Sovinec

Center for Plasma Theory and Computation, University of Wisconsin-Madison, Madison, Wisconsin 53706, USA

(Received 25 November 2008; published 11 June 2009)

Recent ideal magnetohydrodynamic (MHD) theory predicts that a perturbation evolving from a linear ballooning instability will continue to grow exponentially in the intermediate nonlinear phase at the same linear growth rate. This prediction is confirmed in ideal MHD simulations. When the Lagrangian compression, a measure of the ballooning nonlinearity, becomes of the order of unity, the intermediate nonlinear phase is entered, during which the maximum plasma displacement amplitude as well as the total kinetic energy continues to grow exponentially at the rate of the corresponding linear phase.

DOI: 10.1103/PhysRevLett.102.235003 PACS numbers: 52.30.Cv, 52.35.Mw, 52.35.Py, 52.65.Kj

The ballooning instability is a pressure gradient driven mode in magnetized plasma that is localized in the unfavorable curvature regions of magnetic field lines [1–3]. The ballooning instability is a ubiquitous, fundamental process [4] that is involved in many phenomena in natural and laboratory magnetized plasmas with high β values. Here, β is the ratio of plasma and magnetic pressures. Relative to other magnetohydrodynamic (MHD) instabilities (e.g., [5,6]), the nonlinear behavior of ballooning instability is less well understood. There is renewed interest in nonlinear ballooning due to its possible roles in edge localized modes (ELMs) in tokamaks [7–9] and the substorm onset process in Earth's magnetotail [10–12]. Early reduced MHD simulations of high-β tokamak plasmas indicate the formation of a singular current sheet in the final nonlinear state of a ballooning instability which had evolved from a linear mode with very low toroidal mode number n ($n = 1$) [13]. More recently, 3D resistive MHD simulations of nonlinear ballooning instability were applied to model high-β disruptions in tokamaks [14,15]. Analytical theory has been developed for nonlinear ballooning growth of a marginally unstable configuration in the early nonlinear regime [16–18]. Analytical theory of the intermediate nonlinear regime of ballooning instability has been developed lately to better understand simulations and experiments [19–21].

The onset of type-I ELMs in tokamaks is well correlated to the breaching of linear ideal MHD ballooning instability boundaries [9]. Filamentary structures and their localization in the unfavorable curvature region of the tokamak edge have been routinely observed in striking optical images from recent Mega Amp Spherical Tokamak (MAST) experiments [22–24]. These filamentary structures are often associated with the structure of linear ballooning instabilities due to their strong resemblance. However, these filaments are relatively long lived and persist well into the nonlinear stage of evolution. The physics mechanism underlying such a close connection between the nonlinear filamentary structures and the nascent linear instabilities is not obvious.

Our recent theory and simulations of nonlinear ballooning instability may provide a more rigorous interpretation of such a phenomenological connection. As predicted from a recent nonlinear ideal MHD theory [21], a perturbation evolving from a linear ballooning instability will continue to maintain its linear mode structure during the intermediate nonlinear phase. Consequentially, the mode continues to grow exponentially in the nonlinear regime with the same growth rate as the linear mode. The existence of such an exponential nonlinear growth phase has been confirmed in our ideal MHD simulations, which is the focus of this Letter.

Different phases of ELM evolution may relate to different linear and nonlinear regimes of ballooning instability. To describe the different nonlinear phases, we introduce two small parameters given by

$$n^{-1} = \frac{k_\parallel}{k_\perp} \ll 1, \qquad \varepsilon = \frac{|\boldsymbol{\xi}|}{L_{\mathrm{eq}}} \ll 1. \tag{1}$$

Here, $k_\parallel$ and $k_\perp$ are the dominant wave numbers of the perturbation parallel to and perpendicular to the equilibrium magnetic field, respectively; $\boldsymbol{\xi}$ is the plasma displacement produced by instability, and L_{eq} is the equilibrium scale length (which is used later as the normalization length in our theory).

The linear structure and growth rates of ballooning instabilities can be determined using an asymptotic expansion of the linearized ideal MHD equation in terms of n^{-1} [2,3,25]. The mode structure in the fastest varying direction perpendicular to the magnetic field is given by n^{-1}, which is the scale of the dominant wavelength. At lowest order in n^{-1}, the ballooning mode is described by two coupled one-dimensional ordinary differential equations along each field line, which together with proper boundary conditions, determines the local eigenfrequency or local growth rate as well as the local mode structure along the equilibrium magnetic field as a function of magnetic flux surface, field line, and radial wave number. At higher order in n^{-1}, a global eigenmode equation, the envelope equa-

tion, which uses information from the local mode calculations, governs the global growth rate and mode structure across magnetic surfaces. In axisymmetric equilibria, the global growth rate is given by the most unstable value of the local growth rate with stabilizing corrections of order n^{-1}. As shown earlier [16–20] and in this work, the properties of linear ballooning instability are crucial to the construction and understanding of the theory of nonlinear ballooning instability.

The perturbation amplitude of the nonlinear ballooning mode, measured by ε ($\sim|\boldsymbol{\xi}|$), can be compared to the characteristic spatial scales of its linear mode structure. In the early nonlinear regime, the filament scale $|\boldsymbol{\xi}|$ across the magnetic flux surface is comparable to the mode width λ_α in the most rapidly oscillating direction, $|\boldsymbol{\xi}| \sim \lambda_\alpha \sim n^{-1}$ [16–18]. In this regime, the nonlinear convection across the flux surface is small relative to the mode width λ_Ψ in that direction. The dominant effect of the nonlinearities is to modify the radial envelope equation describing mode evolution across the magnetic surface. Here, Ψ and α are the flux and field line labels, respectively, which are later used to define the equilibrium magnetic field. As the mode continues to grow, it enters the intermediate nonlinear regime, in which $|\boldsymbol{\xi}| \sim \lambda_\Psi \sim n^{-1/2}$; the plasma displacement across the magnetic flux surface becomes of the same order as the mode width in the same direction [19,20]. In this regime, effects due to convection and compression are no longer small. Nonlinearities due to convection and compression, together with nonlinear line-bending forces, directly modify the ''local'' mode evolution along the magnetic field line. In the late nonlinear regime, the ballooning filament growth may exceed the scale of the pedestal width. Eventually, these ballooning filaments could detach from edge plasma and propagate into the scrape-off-layer region, as indicated from recent experiment [23]. In this work, we consider the physics of the intermediate nonlinear phase and leave discussion of the late nonlinear regime for subsequent work.

The linear to early nonlinear regime of the ballooning instability of the pedestal may correspond to the initial development of type-I ELMs. Earlier theory attempted to explain the collapse onset phase of ELMs by invoking a finite timelike singularity associated with the early nonlinear ballooning instability of a marginally unstable configuration (''Cowley-Artun'' regime) [16–18]. Such a scenario, however, has yet to be confirmed by direct MHD simulations, possibly due to the rather limited range of validity for that regime. In contrast, there is a good agreement between the solutions of the intermediate nonlinear regime equations and results from direct MHD simulations for both the case of a line-tied g mode [20] and the ballooning instability of a tokamak (as shown in this Letter). This regime could become particularly relevant for application to ELMs as the width of the transport barrier (or pedestal) region is comparable to the mode width of the dominant ballooning instability.

In the following, the theory of the intermediate nonlinear regime of the ballooning instability is briefly reviewed. A detailed calculation can be found in [21]. We then describe the comparison between the theory prediction and direct MHD simulations of the ballooning instability in a tokamak.

The nonlinear theory of ballooning modes can be conveniently developed in the Lagrangian formulation of the ideal MHD model [26]

$$\frac{\rho_0}{J}\nabla_0\mathbf{r}\cdot\frac{\partial^2\boldsymbol{\xi}}{\partial t^2} = -\nabla_0\left[\frac{p_0}{J^\gamma}+\frac{(\mathbf{B}_0\cdot\nabla_0\mathbf{r})^2}{2J^2}\right] + \nabla_0\mathbf{r}\cdot\left[\frac{\mathbf{B}_0}{J}\cdot\nabla_0\left(\frac{\mathbf{B}_0}{J}\cdot\nabla_0\mathbf{r}\right)\right] \quad (2)$$

where $\mathbf{r}(\mathbf{r}_0, t) = \mathbf{r}_0 + \boldsymbol{\xi}(\mathbf{r}_0, t)$, $\nabla_0 = \partial/\partial\mathbf{r}_0$, $J(\mathbf{r}_0, t) = |\nabla_0\mathbf{r}|$. Here, $\mathbf{r}_0$ denotes the initial location of each plasma element in the equilibrium, $\boldsymbol{\xi}$ is the plasma displacement from the initial location, and $J(\mathbf{r}_0, t)$ is the Jacobian for the Lagrangian transformation from $\mathbf{r}_0$ to $\mathbf{r}(\mathbf{r}_0, t)$; ρ_0, p_0, and $\mathbf{B}_0$ are the equilibrium mass density, pressure, and magnetic field, respectively. We consider a general magnetic configuration that can be described by $\mathbf{B}_0 = \nabla_0\Psi_0\times\nabla_0\alpha_0$ in a nonorthogonal Clebsch coordinate system (Ψ_0, α_0, l_0), where Ψ_0 is the magnetic flux label, α_0 the field line label, and l_0 the measure of field line length. The corresponding coordinate Jacobian is given by $(\nabla_0\Psi_0\times\nabla_0\alpha_0\cdot\nabla_0 l_0)^{-1} = |\mathbf{B}_0|^{-1}$.

The intermediate nonlinear regime is defined by the ordering $\varepsilon\sim\mathcal{O}(n^{-1/2})$ [19,20]. In this regime, the plasma displacement $\boldsymbol{\xi}$ can be expanded as a single series in $n^{-1/2}$

$$\boldsymbol{\xi}(\sqrt{n}\Psi_0, n\alpha_0, l_0, t) = \sum_{j=1}^{\infty} n^{-j/2}\left(\mathbf{e}_\perp\xi^\Psi_{j/2} + \frac{\mathbf{e}_\wedge}{\sqrt{n}}\xi^\alpha_{(j+1)/2} + \mathbf{B}\xi^{\|}_{j/2}\right) \quad (3)$$

where $\mathbf{e}_\perp = (\nabla_0\alpha_0\times\mathbf{B})/B^2$, $\mathbf{e}_\wedge = (\mathbf{B}\times\nabla_0\Psi_0)/B^2$. Here and subsequently, we drop the subscript ''0'' in the equilibrium MHD fields ρ_0, p_0, and $\mathbf{B}_0$ for convenience. The spatial structure of the perturbation quantities is determined by the conventional ballooning theory ordering; the plasma displacement $\boldsymbol{\xi}$ and the Lagrangian Jacobian J are functions of the normalized coordinates (Ψ, α, l), where $\Psi = \sqrt{n}\Psi_0$, $\alpha = n\alpha_0$, $l = l_0$.

Evolution equations for the ideal MHD plasma displacement in the intermediate nonlinear regime can be obtained using a perturbation theory in $\varepsilon\sim n^{-1/2}\ll 1$. These equations are given by [21]

$$[\Psi + \xi^\Psi_{1/2}, \rho|\mathbf{e}_\perp|^2\partial_t^2\xi^\Psi_{1/2} - \mathcal{L}_\perp(\xi^\Psi_{1/2}, \xi^{\|}_{1/2})] = 0, \quad (4)$$

$$\rho B^2\partial_t^2\xi^{\|}_{1/2} - \mathcal{L}_{\|}(\xi^\Psi_{1/2}, \xi^{\|}_{1/2}) = 0. \quad (5)$$

where $\partial_t = (\partial/\partial t)_{\mathbf{r}_0}$, $[A, B]\equiv\partial_\Psi A\partial_\alpha B - \partial_\alpha A\partial_\Psi B$, $\mathcal{L}_\perp$ ($\mathcal{L}_{\|}$) is the perpendicular (parallel) component of the local linear ballooning operator [17,21]. The structure of Eq. (4)

indicates that the solution satisfies the following general form

$$\rho|\mathbf{e}_\perp|^2\partial_t^2\xi^\Psi_{1/2} = \mathcal{L}_\perp(\xi^\Psi_{1/2}, \xi^\parallel_{1/2}) + N(\Psi + \xi^\Psi_{1/2}, l, t), \quad (6)$$

where $N(\tilde{\Psi}, l, t)$ is a function of the distorted flux function $\tilde{\Psi} = \Psi + \xi^\Psi_{1/2}$, field line coordinate l and time. A particular choice is $N(\tilde{\Psi}, l, t) = 0$, which implies that solutions of the linear local ballooning mode equations continue to be solutions of the nonlinear ballooning Eqs. (4) and (5) formally. The nonlinear contributions to Eqs. (4) and (5) vanish for any nonlinear solution that assumes the linear ballooning mode structure in Lagrangian coordinates. As a consequence, global quantities of the perturbation, such as the maximum magnitude of plasma displacement and the total kinetic energy, grow exponentially at the growth rate of the linear phase, even in the intermediate nonlinear stage.

This theoretical prediction has been confirmed in recent direct MHD simulations of nonlinear ballooning instability in a tokamak using the NIMROD code [27]. The simulation starts with a small perturbation to a toroidal tokamak equilibrium generated with the Equilibrium and Stability Code (ESC) solver [28] (Fig. 1). The equilibrium has a circular shaped boundary with major radius $R_0 = 3$ and minor radius $a = 1$ (all quantities are in SI units). The pressure profile is pedestal-like: $\mu_0 p(x) = p_p + h_p \tanh[(x_p - x)/L_p]$, where $p_p = 0.045$, $h_p = 0.044$, $x_p = 0.7$, $L_p = 0.05$, $x = \sqrt{\Psi_T/\Psi_{Ta}}$, and Ψ_T (Ψ_{Ta}) is the toroidal flux (at boundary). The safety factor q is monotonically increasing: $q = q_0[1 + (q_a/q_0 - 1)x^4]$, with $q_0 = 1.05$, $q_a = 3$. The magnetic field at the magnetic axis is $B_0 = 1$. The initial perturbation is dominated by an $n = 15$ Fourier component in the toroidal direction. The perturbation is advanced using the standard set of ideal MHD equations (with resistivity $\eta = 0$) in the NIMROD simulation [27]. We also advance the ideal MHD plasma displacement vector as an extra field in Eulerian coordinates using

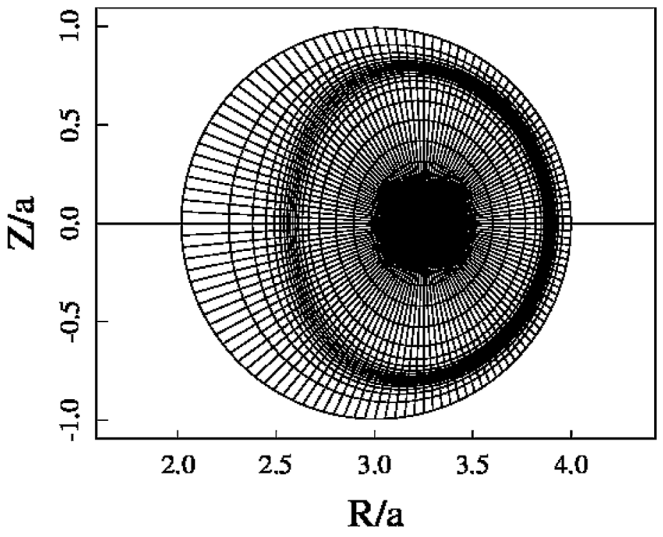

FIG. 1. The finite element mesh of poloidal domain based on a tokamak equilibrium generated using the ESC solver. R and Z are the cylindrical coordinates; a is the minor radius. The rings of grid lines approximate contours of constant equilibrium pressure. The mesh has 20×128 (radial $\times$ poloidal) grid points with fifth order polynomial basis functions in each direction.

$$\partial_t\boldsymbol{\xi}(\mathbf{r}, t) + \mathbf{u}(\mathbf{r}, t)\cdot\nabla\boldsymbol{\xi}(\mathbf{r}, t) = \mathbf{u}(\mathbf{r}, t) \quad (7)$$

where $\mathbf{u}(\mathbf{r}, t)$ is the velocity field, $\partial_t = (\partial/\partial t)_\mathbf{r}$, and $\nabla = \partial/\partial\mathbf{r}$. We then calculate the Lagrangian compression $\nabla_0\cdot\boldsymbol{\xi}$ from the Eulerian tensor $\nabla\boldsymbol{\xi}$ using the identity

$$\nabla_0\cdot\boldsymbol{\xi} = \mathrm{Tr}(\nabla_0\boldsymbol{\xi}) = \mathrm{Tr}[(\mathbf{I} - \nabla\boldsymbol{\xi})^{-1}\cdot\nabla\boldsymbol{\xi}]. \quad (8)$$

Both the maximum plasma displacement $|\boldsymbol{\xi}|_{\max}$ and the maximum Lagrangian compression $(\nabla_0\cdot\boldsymbol{\xi})_{\max}$ of the entire simulation domain evolve at the same linear growth rate during the phase $10\tau_A \lesssim t \lesssim 30\tau_A$. Here, the Alfvén time $\tau_A = a\sqrt{\mu_0\rho}/B_0$, where ρ is the mass density. When the Lagrangian compression $(\nabla_0\cdot\boldsymbol{\xi})_{\max}$ becomes of order unity, the perturbation has evolved into the intermediate nonlinear phase, which is characterized by the ordering

$$\boldsymbol{\xi}\cdot\nabla_0 \sim \nabla_0\cdot\boldsymbol{\xi} \sim \lambda_\Psi^{-1}\xi^\Psi + \lambda_\alpha^{-1}\xi^\alpha \sim 1. \quad (9)$$

However, the maximum plasma displacement itself continues to grow exponentially with the same growth rate of the linear phase of the mode well into the intermediate nonlinear phase. This behavior is demonstrated in Fig. 2, which is consistent with the special solution of the analytic theory [21]. The sudden enhanced growth of the Lagrangian compression $\nabla_0\cdot\boldsymbol{\xi}$ in Fig. 2 above the intermediate nonlinear regime may reflect the fact that the matrix $(\mathbf{I} - \nabla\boldsymbol{\xi})$ may become nearly singular during the nonlinear phase, even though the Eulerian compression $\nabla\cdot\boldsymbol{\xi}$ remains finite. For the case shown in Fig. 2, the tokamak minor radius is $a = 1$, and the pressure pedestal width is $L_{\mathrm{ped}} \sim 0.1$. As the Lagrangian compression $(\nabla_0\cdot\boldsymbol{\xi})_{\max} \gg 1$, the mode passes through the intermediate nonlinear phase, and the maximum plasma displacement $|\boldsymbol{\xi}|_{\max}$ surpasses the pedestal scale length L_{ped}. At this point, the analytical theory developed in Ref. [21] no longer applies.

In summary, direct numerical simulations of the full ideal MHD model have confirmed the prediction from a recently developed analytic theory for the ballooning mode growth in the intermediate nonlinear regime. Both theory and simulations have demonstrated that a perturbation that evolves from a linear ballooning instability can continue to grow exponentially at the same growth rate in the intermediate nonlinear stage, and maintain the filamentary mode structure of the corresponding linear phase described in Lagrangian coordinates. This may explain why in experiments, the nonlinear type-I ELM filaments strongly resemble the structure of a linear ballooning mode, and linear analyses have often been able to match and predict the observed mode structures of ELMs [9,29]. It is likely that those type-I ELM filaments observed in optical images

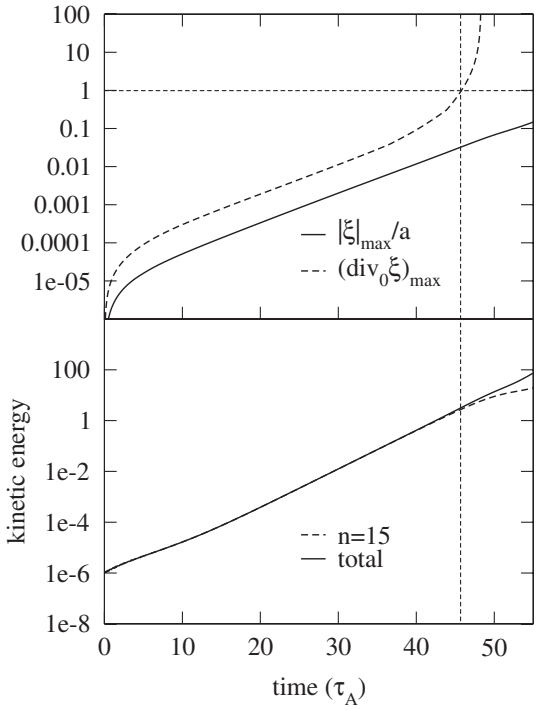

FIG. 2. Top: Growth of the maximum amplitude of plasma displacement $|\boldsymbol{\xi}|_{\max}$ normalized by minor radius a (solid line) and growth of the maximum Lagrangian compression $(\nabla_0 \cdot \boldsymbol{\xi})_{\max}$ (dashed line) calculated from a NIMROD simulation. The time is normalized by the Alfvén time τ_A. The horizontal and vertical dashed lines mark the intermediate nonlinear regime as determined by the ordering $\nabla_0 \cdot \boldsymbol{\xi} \sim 1$. Bottom: Growth of the total kinetic energy (solid line) and the kinetic energy of the $n = 15$ Fourier component (dashed line). The vertical dashed line marks the intermediate nonlinear regime in time. Both vertical axes are in logarithmic scales.

are in fact consequences of the nonlinear evolution of ballooning instability, whose close connection to its linear mode properties can indeed be more rigorously established. Such an insight from theory could have a practical significance as it allows a convenient and accurate interpretation of the nonlinear filaments observed in ELM experiments as well as for future designs of active ELM control.

Our analytical model focuses on the nonlinear growth of the ballooning filament in the ideal MHD regime. This study is an important step toward the construction of a more relevant two-fluid MHD model for the dynamics of nonlinear ballooning and ELM filaments. The two-fluid effects on nonlinear ballooning instability have yet to be fully elucidated and will be the subject of future work.

This research is supported by U.S. Department of Energy under Grants No. DE-FG02-86ER53218 and No. DE-FC02-08ER54975. Computations were performed in NERSC, which is supported by U.S. Department of Energy under Contract No. DE-AC03-76SF00098. The authors are grateful for discussions with J. D. Callen, S. C. Cowley, and P. B. Snyder, and for contributions to code development from the NIMROD team.

[1] B. Coppi, Phys. Rev. Lett. **39**, 939 (1977).
[2] J. W. Connor, R. J. Hastie, and J. B. Taylor, Phys. Rev. Lett. **40**, 396 (1978).
[3] R. L. Dewar and A. H. Glasser, Phys. Fluids **26**, 3038 (1983).
[4] E. Hameiri, Commun. Pure Appl. Math. **38**, 43 (1985).
[5] P. H. Rutherford, Phys. Fluids **16**, 1903 (1973).
[6] M. N. Rosenbluth, R. Y. Dagazian, and P. H. Rutherford, Phys. Fluids **16**, 1894 (1973).
[7] C. C. Hegna, J. W. Connor, and R. J. Hastie *et al.*, Phys. Plasmas **3**, 584 (1996).
[8] J. W. Connor, Plasma Phys. Controlled Fusion **40**, 531 (1998).
[9] P. B. Snyder, H. R. Wilson, and J. R. Ferron *et al.*, Phys. Plasmas **9**, 2037 (2002).
[10] A. Roux, S. Perraut, and P. Robert *et al.*, J. Geophys. Res. **96**, 17697 (1991).
[11] A. Bhattacharjee, Z. W. Ma, and X. Wang, Geophys. Res. Lett. **25**, 861 (1998).
[12] P. Zhu, C. R. Sovinec, and C. C. Hegna *et al.*, J. Geophys. Res. **112**, A06222 (2007).
[13] D. A. Monticello, W. Park, and S. Jardin *et al.*, *Eighth International Conference on Plasma Physics and Controlled Nuclear Fusion* (IAEA, Vienna, 1981), Vol. 1, pp. 227–235, paper IAEA-CN-38/J-1.
[14] W. Park, E. D. Fredrickson, and A. Janos *et al.*, Phys. Rev. Lett. **75**, 1763 (1995).
[15] R. G. Kleva and P. N. Guzdar, Phys. Rev. Lett. **80**, 3081 (1998).
[16] S. C. Cowley and M. Artun, Phys. Rep. **283**, 185 (1997).
[17] O. A. Hurricane, B. H. Fong, and S. C. Cowley, Phys. Plasmas **4**, 3565 (1997).
[18] H. R. Wilson and S. C. Cowley, Phys. Rev. Lett. **92**, 175006 (2004).
[19] P. Zhu, C. C. Hegna, and C. R. Sovinec, Phys. Plasmas **13**, 102307 (2006).
[20] P. Zhu, C. C. Hegna, and C. R. Sovinec *et al.*, Phys. Plasmas **14**, 055903 (2007).
[21] P. Zhu and C. C. Hegna, Phys. Plasmas **15**, 092306 (2008).
[22] A. Kirk, B. Koch, and R. Scannell *et al.*, Phys. Rev. Lett. **96**, 185001 (2006).
[23] A. Kirk, G. F. Counsell, and G. Cunningham *et al.*, Plasma Phys. Controlled Fusion **49**, 1259 (2007).
[24] N. B. Ayed, A. Kirk, and B. Dudson *et al.*, Plasma Phys. Controlled Fusion **51**, 035016 (2009).
[25] J. W. Connor, R. J. Hastie, and J. B. Taylor, Proc. R. Soc. A **365**, 1 (1979).
[26] D. Pfirsch and R. N. Sudan, Phys. Fluids B **5**, 2052 (1993).
[27] C. Sovinec, A. Glasser, and D. Barnes *et al.*, J. Comput. Phys. **195**, 355 (2004).
[28] L. E. Zakharov and A. Pletzer, Phys. Plasmas **6**, 4693 (1999).
[29] P. B. Snyder, H. R. Wilson, and X. Q. Xu, Phys. Plasmas **12**, 056115 (2005).